BRAIN
ORIGINAL ARTICLE

Inhibiting mitochondrial fission rescues degeneration in hereditary spastic paraplegia neurons

Zhenyu Chen,[1,2] Eric Chai,[1] Yongchao Mou,[1,2] Ricardo H. Roda,[3,4] (iD)Craig Blackstone[3,5,6] and (iD)Xue-Jun Li[1,2]

Hereditary spastic paraplegias are characterized by lower limb spasticity resulting from degeneration of long corticospinal axons. SPG11 is one of the most common autosomal recessive hereditary spastic paraplegias, and the SPG11 protein spatacsin forms a complex with the SPG15 protein spastizin and heterotetrameric AP5 adaptor protein complex, which includes the SPG48 protein AP5Z1. Using the integration-free episomal method, we established SPG11 patient-specific induced pluripotent stem cells (iPSCs) from patient fibroblasts. We differentiated SPG11 iPSCs, as well as SPG48 iPSCs previously established, into cortical projection neurons and examined protective effects by targeting mitochondrial dynamics using P110, a peptide that selectively inhibits mitochondrial fission GTPase Drp1. P110 treatment mitigates mitochondrial fragmentation, improves mitochondrial motility, and restores mitochondrial health and ATP levels in SPG11 and SPG48 neurons. Neurofilament aggregations are increased in SPG11 and SPG48 axons, and these are also suppressed by P110. Similarly, P110 mitigates neurofilament disruption in both SPG11 and SPG48 knockdown cortical projection neurons, confirming the contribution of hereditary spastic paraplegia gene deficiency to subsequent neurofilament and mitochondrial defects. Strikingly, neurofilament aggregations in SPG11 and SPG48 deficient neurons double stain with ubiquitin and autophagy related proteins, resembling the pathological hallmark observed in SPG11 autopsy brain sections. To confirm the cause-effect relationship between the *SPG11* mutations and disease phenotypes, we knocked-in SPG11 disease mutations to human embryonic stem cells (hESCs) and differentiated these stem cells into cortical projection neurons. Reduced ATP levels and accumulated neurofilament aggregations along axons are observed, and both are mitigated by P110. Furthermore, rescue experiment with expression of wild-type *SPG11* in cortical projection neurons derived from both SPG11 patient iPSCs and SPG11 disease mutation knock-in hESCs leads to rescue of mitochondrial dysfunction and neurofilament aggregations in these SPG11 neurons. Finally, in SPG11 and SPG48 long-term cultures, increased release of phosphoNF-H, a biomarker for nerve degeneration, is significantly reduced by inhibiting mitochondrial fission pharmacologically using P110 and genetically using Drp1 shRNA. Taken together, our results demonstrate that impaired mitochondrial dynamics underlie both cytoskeletal disorganization and axonal degeneration in SPG11 and SPG48 neurons, highlighting the importance of targeting these pathologies therapeutically.

1 Department of Biomedical Sciences, University of Illinois College of Medicine Rockford, Rockford, IL 61107, USA
2 Department of Bioengineering, University of Illinois at Chicago, Chicago, IL 60607, USA
3 Cell Biology Section, Neurogenetics Branch, National Institute of Neurological Disorders and Stroke, National Institutes of Health, Bethesda, MD 20892, USA
4 Department of Neurology, Johns Hopkins University of Medicine, Baltimore, MD 21205, USA
5 Movement Disorders Division, Department of Neurology, Massachusetts General Hospital, Boston, MA 02114, USA
6 MassGeneral Institute for Neurodegenerative Disease, Massachusetts General Hospital, Charlestown, MA 02129, USA

Correspondence to: Xue-Jun Li, PhD Department of Biomedical Sciences University of Illinois College of Medicine
Rockford Rockford, IL 61107, USA E-mail: xjli23@uic.edu

Correspondence may also be addressed to: Craig Blackstone, MD, PhD
MassGeneral Institute for Neurodegenerative Disease
Massachusetts General Hospital
Charlestown, MA 02129, USA
E-mail: cblackstone@mgh.harvard.edu

Introduction

Hereditary spastic paraplegias (HSPs) are a large, diverse group of inherited neurological diseases with the unifying feature of progressive lower limb spasticity, caused by length-dependent axonopathy of long corticospinal tract axons.[1–3] Over 80 genetic loci haven been identified to be associated with spastic paraplegias (SPG1–83, plus others).[4–6] Based on genetic inheritance, HSPs are classified into dominant, recessive, and X-linked forms; *de novo* and mitochondrial DNA mutations have also been described. SPG11 is a common autosomal recessive HSP caused by biallelic loss-of-function mutations in the *SPG11* gene that encodes the large spatacsin protein.[7,8] Spatacsin is part of a multiprotein complex with the SPG15 protein spastizin and the AP5 adaptor complex that includes the SPG48 protein AP5Z1.[9] SPG11 patients have a number of other neurological findings in addition to lower extremity spasticity, such as cognitive impairment, early-onset parkinsonism, peripheral neuropathy, retinal degeneration, and cerebellar ataxia. Plus, many patients have thin corpus callosum and white matter changes described as 'ears of the lynx'.[7,10]

Knockdown of spatacsin (*spg11*) in zebrafish leads to impaired axonal outgrowth and locomotor impairment, prefiguring involvement in axonal development and maintenance.[11] Spg11 knockout mice develop early-onset motor impairment and cognitive deficits, with loss of neurons in several brain regions and accumulation of dystrophic axons in the corticospinal tract.[12] At the cellular level, loss of spatacsin leads to accumulation of lipids within lysosomes as a result of defective clearance,[12] and accumulations of granular lysosome-like structures and neurofilament aggregations are observed in post-mortem SPG11 brain sections.[13] However, pathways relevant for amelioration of SPG11 related phenotypes have remained elusive.

Studies of neuronal defects in HSP reveal impairments in common cellular activities such as axonal transport, cytoskeletal dynamics, endoplasmic reticulum morphology and endolysosomal and autophagic functions.[14,15] In addition to roles of autophagy and endolysosomal trafficking,[16,17] recent studies have demonstrated that loss of spastizin or AP5Z1 proteins impairs mitochondrial dynamics in cortical neurons derived from SPG15 and SPG48 induced pluripotent stem cells (iPSCs), respectively.[18,19] Imbalanced mitochondrial fission and fusion leads to abnormal mitochondrial morphology, resulting in mitochondrial functional defects and aberrant cellular homeostasis.[20,21] By inhibiting the mitochondrial fission GTPase dynamin-related protein 1 (Drp1),[22,23] fragmentation of mitochondria in SPG15 and SPG48

neurons can be suppressed and mitochondria health improved.[24] Moreover, axonal outgrowth defects in these neurons are rescued, indicating a possible contribution of impaired mitochondrial dynamics to axonal outgrowth defects in HSP.[24] Whether SPG11 mutations lead to mitochondrial dysfunction and how impaired mitochondrial dynamics results in axonal degeneration in long-term HSP neuron cultures remain unclear.

A key barrier to studying neurological diseases is the difficulty in obtaining high-quality patient neurons. With the development of iPSC technology, patient-specific iPSCs provide a unique source to generate various types of neural cells for the study of neurodegenerative diseases in which certain types of neurons are selectively affected.[25–28] To investigate the role of mitochondrial dynamics in SPG11 pathogenesis, we generated patient-specific SPG11 iPSCs and differentiated SPG11 and control iPSCs into cortical projection neuron. In complementary studies, we also generated SPG11 disease mutation knock-in hESCs using CRISPR/cas9-mediated gene editing. We then examined the effects of P110, a peptide that selectively inhibits the mitochondrial fission GTPase Drp1, on mitochondrial dysfunction and axonal degeneration in SPG11 neurons.[29] Treatment with P110 restores mitochondrial morphology, motility, and membrane potential and, importantly, rescues axonal and neuronal degeneration in long-term cultures of SPG11 neurons. Similar protective effects of P110 are observed in SPG48 neurons, further supporting the potential use of P110 against nerve degeneration in HSPs. Moreover, the impaired neurofilament organization in these HSP neurons is rescued by restoring mitochondria function using P110, indicating the promising role of mitochondrial fission inhibition in rescuing nerve degeneration by mitigating mitochondrial and cytoskeletal defects in SPG11 and SPG48.

Material and methods

Clinical study and human SPG11 fibroblasts

Clinical evaluation and collection of patient fibroblast cells were performed under an Institutional Review Board-approved clinical research protocol (NINDS protocol 00-N-0043) at the National Institutes of Health Clinical Center. Skin fibroblasts were obtained from a skin punch biopsy of a patient with SPG11 and cultured using standard procedures.

The patient presented to the NIH Clinical Center at age 31. He first noticed difficulty running at age 6, and by 15 he had a clearly abnormal gait. He was still able to play lacrosse early in college, but by age 23 he required a cane to ambulate and had also developed

dysarthria and dysphagia. Over the next several years he became non-ambulatory. He received an intrathecal baclofen pump to control spasticity. On examination, he had very prominent weakness in the lower extremities and increased tone but normal power in the upper extremities. There was no ataxia or rigidity, but pinprick and vibratory sensation were diminished in the feet. Gene testing revealed compound heterozygous, pathogenic frameshift mutations in the SPG11 gene: c.3965delG and c.5769_5770dupT (Fig. 1A).

Generation of human iPSC lines and SPG11 mutation knock-in hESC lines

Human fibroblast cells were cultured in medium containing 90% Dulbecco's modified Eagle medium (DMEM), 10% foetal bovine serum (FBS) and 1× non-essential amino acids (NEAAs). To generate iPSC lines using an episomal protocol, about 2×10^5 fibroblast cells were electroporated with episomal plasmids (Addgene) expressing pluripotency factors (Oct3/4, Sox2, L-Myc, Klf4 and Lin 28).[30] One week later, cells were passaged, and another week later, cells were dissociated and plated on irradiated mouse embryonic fibroblasts (MEFs). Two weeks later, colonies with representative pluripotent morphology were picked up and expanded. After further identification, established iPSCs lines were selected for experiment. Teratoma testing for validating the pluripotency of iPSCs was performed by injecting dissociated iPSCs into severe combined immunodeficient (SCID) mice and then collecting teratomas for histological analysis as described previously.[31]

To generate SPG11 knock-in human embryonic stem cell (hESC) lines, a c.118C>T (p.Gln40X) homozygous mutation was introduced into H9 hESC lines using CRISPR/Cas9-mediated gene editing by the iPSC core at the University of Connecticut Health Center. The nucleotide at the 117 position was changed from G to C to facilitate the gene editing process, and this change did not affect the amino acid sequence. H9 cells were used as isogenic controls. By combining lentiviral infection and RNA interference, we also generated SPG11-knockdown H9 cell lines. The SPG48-knockdown H9 cell line was established in our previous study.[24] Cell lines used in this study are listed in Supplementary Table 1. All experiments involving hESCs and iPSCs were approved by the University of Illinois Embryonic Stem Cell Research Oversight Committee (ESCRO) and IBC. The Institutional Animal Care and Use Committee at the University of Illinois approved animal studies involving teratoma formation.

Human iPSCs and hESCs neural differentiation

Human iPSCs and hESCs were cultured on irradiated MEF with human embryonic stem cell (ESC) medium containing 10 ng/ml basic fibroblast growth factor (b-FGF). IPSCs and ESCs were detached from the feeder layer to form aggregates in ESC medium without b-FGF for 2 days and in human neural induction medium (NIM) for the following 5 days. Next, iPSC and ESC aggregates were plated onto 6-well plates with 10% FBS in NIM for 12 h. NIM was added for another 10 days, with medium changed every other day, in order to generate neuroepithelial cells. Neuroepithelial cells were mechanically detached into suspension culture to form neurospheres, supplemented with NIM with B27, cAMP and insulin-like growth factor 1 (IGF-1) for 10 additional days. At about Day 28, neurospheres were dissociated and plated on poly-ornithine-pretreated and Matrigel-coated coverslips for terminal differentiation; they were cultured in neural differentiation medium (NDM) containing N2, B27, cAMP, IGF-1, brain-derived neurotrophic factor (BDNF) and glial-derived neurotrophic factor (GDNF).[32,33] To test the effects of P110, cells were cultured in medium supplemented with 1 μM P110.

Quantitative reverse transcription PCR

Total RNA was isolated from cells using TRIzol™ reagent (Invitrogen) following manufacturer's instructions. A total of 1 μg of RNA was used to synthesize cDNA using iScriptcDNA Synthesis Kit (Bio-Rad) following manufacturer's parameters. To examine the mRNA expression, qPCR was performed in a 20 μl mixture containing cDNA, primers and 1× SYBR Green PCR Master mix (Applied Biosystems) using the QuantStudio 6 Flex Real-Time PCR System (Applied Biosystems). Expression levels of the mRNA were calculated using the comparative CT method. The following primers were used: SPATACSIN, 5′-CTCCTAGTGTCCTGCCATCTGA-3′ (forward) and 5′-GGCTAGAGAAATGTGGGAGATG-3′ (reverse); DRP1, 5′-AAATCGTCGTAGTGGGAACG-3′ (forward) and 5′-TGGACCAG TTGCAGAATGAG-3′ (reverse); SPATACSIN (C-terminal), 5′-ACACAG ATGTTGCTGCTCAG-3′ (forward) and 5′-ACGAGTTCAGCCACAG TATC-3′ (reverse); GAPDH, 5′-ATGACATCAAGAAGGTGGTG-3′ (forward) and 5′-CATACCAGGAAATGAGCTTG-3′ (reverse). Primer set for SPATACSIN C-terminal was used to examine the expression of SPATACSIN in SPG11 iPSC- and knock-in hESC-derived neural cultures.

Western blotting

Cells were lysed in radioimmunoprecipitation assay (RIPA) buffer with PMSF and proteinase inhibitor cocktails. Samples (20 μg protein) were run on 8% or 10% SDS-PAGE gels, then incubated with primary antibodies in 3% bovine serum albumin (BSA) overnight at 4°C followed by the incubation with secondary antibodies. After adding enhanced chemiluminescence (ECL) substrate, immunoreactivity was revealed using the Bio-Rad ChemiDoc™ MP Imaging System. Primary antibodies included anti-SPG11 (rabbit IgG, Sigma-Aldrich, HPA040412, 1:1000) and anti-β-actin (mouse IgG, Sigma-Aldrich, A5316, 1:5000). Secondary antibodies were HRP-conjugated IgG from Jackson ImmunoResearch, 1:10 000.

Immunocytochemistry

Cells on glass coverslips were fixed with 4% paraformaldehyde for 15 min, followed by several washes with phosphate-buffered saline (PBS). A 0.2% Triton-X solution in PBS was used for permeabilization for 10 min, and 10% donkey serum solution in PBS was used for blocking for 1 h. Cells were incubated with primary antibodies overnight and secondary antibodies for 1 h. Antibodies used included: anti-TRA-1-60 (mouse IgM, Santa Cruz, 1:50); anti-NANOG (goat IgG, R&D Systems, 1:500); anti-SSEA4 (mouse IgG3, DSHB, 1:100); anti-OCT4 (mouse IgG, Santa Cruz, 1:200); anti-CTIP2 (rat IgG, Abcam, 1:2000); anti-NEUN (rabbit IgG, Abcam, 1:500); anti-NF200 (rabbit IgG, Sigma-Aldrich, 1:1000), anti-p-NFH (mouse IgG, Millipore, 1:1000); anti-Tom20 (mouse IgG, Proteintech, 1:500); anti-UCHL1 (Rabbit IgG, Proteintech, 1:500).

For axon outgrowth experiments, neurospheres were dissociated into single cells and plated on Matrigel-coated coverslips. After treatment with or without P110 for 2 days, neurons were fixed and stained with anti-Tau antibody. Axons are defined as the longest neurite which also stains the strongest for Tau as we previously described.[26] Primary neurites are defined as neurites directly coming out of the cell bodies. The number of branches is the total number of primary neurites of the cell. At least 70 cells from three coverslips were selected blindly per group and was quantified using
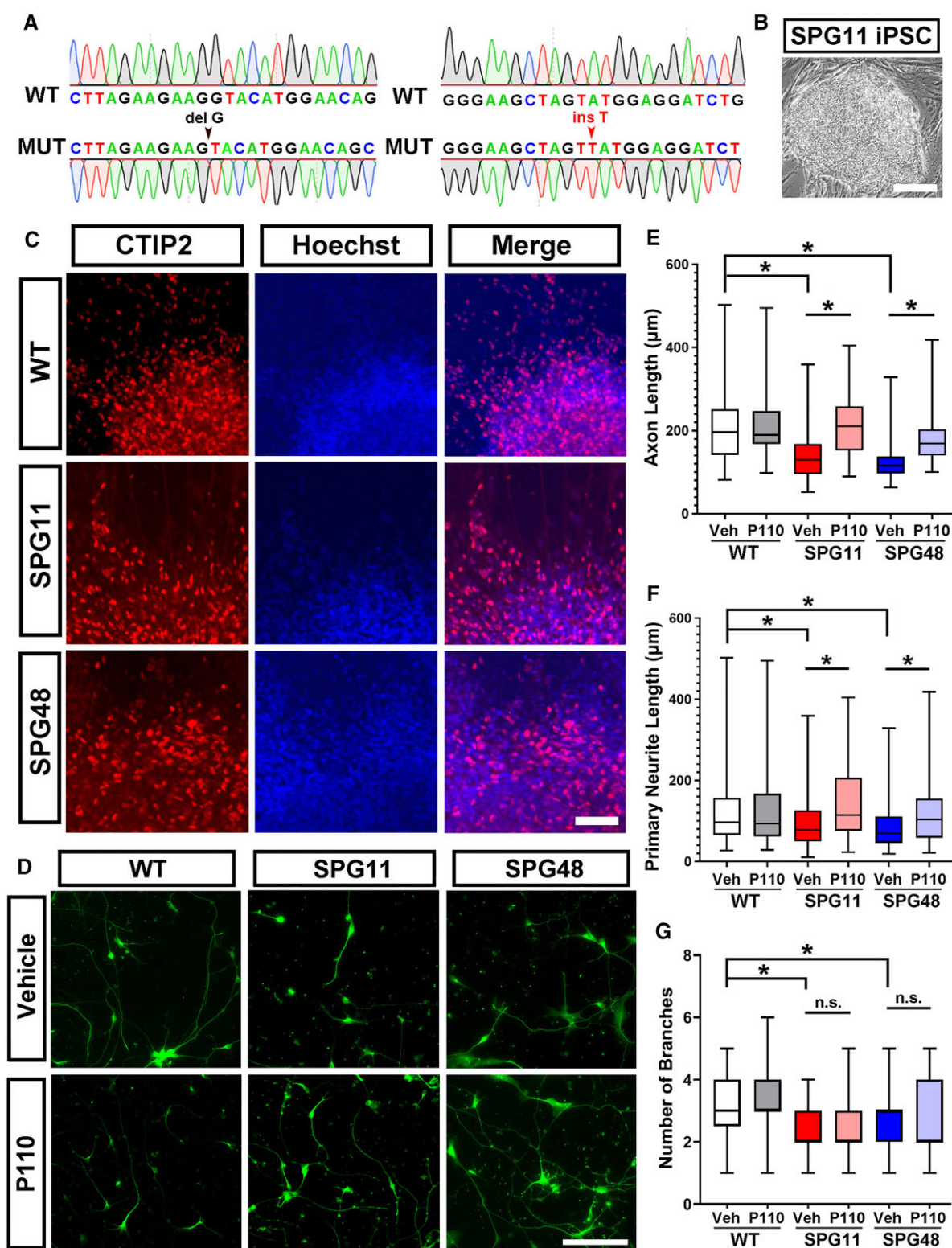
Figure 1 Morphological characterization of SPG11 and SPG48 cortical projection neurons and effects of mitochondrial fission inhibitor P110. (A) DNA sequencing electropherograms confirm the presence of biallelic mutations of SPG11, c.3965delG and c.5769_5770dupT, in iPSCs **(B)** derived from the SPG11 patient. **(C)** Immunostaining showing the generation of CTIP2+ cortical projection neurons from wild-type (WT) control, SPG11, and SPG48 iPSCs. Blue indicates Hoechst-stained nuclei. Scale bar = 100 μm. **(D)** To analyse neurite outgrowth of these cortical projection neurons, Tau immunostaining was performed. Axons were strongly stained for Tau. Using ImageJ, axon length **(E)**, primary neurite length **(F)**, and number of branches **(G)** were analysed and compared between groups treated with vehicle or P110. Data are presented using box and whisker plots, with all elements (median, interquartile interval, minimum, maximum) shown. At least 70 cells from three coverslips were analysed per group. Scale bars = 200 **(B)** and 100 μm **(C** and **D)**. Dunnett's test after ANOVA was used to compare multiple groups with the wild-type group. Two-sided *t*-tests were used to examine differences between vehicle- and P110-treated groups. *P < 0.05; n.s. = not significant.

ImageJ software.[26] To quantify the proportion of CTIP2 and NEUN-expressing cells, a Keyence BZ-X800 fluorescence microscope with ×40 objective was used to capture images after immunostaining of coverslips. At least three fields of each coverslip were chosen and counted (three coverslips each group) using ImageJ software by an observer blinded to the experimental conditions.

Mitochondrial live-cell imaging

Neurospheres were plated onto glass bottom 35 mm dishes. Before imaging, cells were treated with 25 nM MitoTracker Red CMXRos (Invitrogen). Then, cells were washed three times with imaging medium, and the dish was placed into a live-cell imaging chamber at 37°C and 5% CO_2. Axons were identified using morphological characteristics (i.e. constant thin diameter, long neurites, no proximal branching, and direct emergence from the cell body), followed by live-cell imaging as previously described.[34,35] Briefly, images of mitochondria along axons were acquired every 5 s for a total of 5 min. Quantitation of the movement of each mitochondrion was performed using ImageJ software by an analyser who was blind to experimental conditions. After tracing each mitochondrion, kymographs of mitochondrial movement were generated (x-axis represents position along axons and y-axis represents time). A minimum of 120 mitochondria from three independent experiments were analysed per group. The velocity of mitochondria showing any movement at the anterograde or retrograde direction[36] was examined. Since mitochondria move more frequently in the anterograde direction in our cultures, the number of anterograde mitochondria is more than that in the retrograde direction. Motile mitochondria are defined as moving more than ~5 μm forward or backward from the origin during the recording period (≥0.016 μm/s).[35,37] Multiple transport parameters including average velocity of mitochondria, the percentage of motile mitochondria, and the frequency of motile mitochondria in both anterograde and retrograde directions were calculated and compared between groups.

Measurement of mitochondrial membrane potential

Mitochondrial membrane potential measurements were based on the fluorescent dye tetramethylrhodamine methyl ester (TMRM, Invitrogen), as previously reported.[24] Cells growing on 35 mm glass bottom dishes were washed three times with imaging medium (136 mM NaCl, 25 mM KCl, 2 mM $CaCl_2$, 1.3 mM $MgCl_2$, 10 mM HEPES, 10 mM glucose, pH 7.4), then incubated with 10 nM TMRM in imaging medium for 45 min at room temperature in the dark. Live-cell imaging was performed as previously described.[34] Randomly selected fields were imaged every 15 s for a total of 300 s. After TMRM imaging, mitochondrial uncoupler FCCP was added at a final concentration of 1 μM, and images were taken every 15 s for a total of 180 s. Images were analysed using MetaMorph, and fluorescence intensities were calculated by subtracting background intensities from initial read-outs.

Measurement of ATP levels

ATP levels were measured using the Luminescent ATP Detection Assay Kit (Abcam, ab113849), according to the manufacturer's protocol. Cultures were dissociated and about 5×10^4 neurons were harvested to perform the assay. After lysis of the cells and addition of luciferase enzyme and substrate, luminescence was measured using a BioTek Synergy2 Multi-Mode Microplate Reader.

Caspase 3/7 activity assay

Caspase 3/7 activities were measured using the Caspase-Glo 3/7 Assay's (Promega) protocol. About 5000 cells were dissociated into single cells and mixed with 50 μl caspase 3/7 reagent in one well of a 96-well plate. After 1 h at room temperature, luminescence was measured using a BioTek Synergy2 Multi-Mode Microplate Reader.

pNF-H ELISA

Medium from neurons at 12 weeks of culture was collected and concentrated to 100 μl with 100 KD Centrifugal Filter Units (Millipore). Samples were then assessed using pNF-H ELISA Version 1 kit (EnCor). Final absorbance was read at 450 nm with a BioTek Synergy2 Multi-Mode Microplate Reader.

Lentiviral production and infection

To express wild-type SPG11 for the rescue experiments, lentiviral plasmid containing the wild-type (WT) full-length SPG11 (E3411, pReceiver-Lv165-EF1α-SPG11-IRES-GFP) was constructed (GeneCopoeia™). To generate lentiviral particles, the Lenti-SPG11 plasmid (or Lenti-GFP plasmid, as control) together with lentivirus packaging plasmids (i.e. pMD2.G and psPAX2) were co-transfected into HEK293T cells using calcium-phosphate precipitation protocol. Viral particles were concentrated through ultracentrifugation at 20 000g for 3 h. Viral particles were then resuspended, aliquoted, and utilized to infect neurons for further analysis.

Statistical analysis

Statistical significance of mean values among multiple sample groups was analysed using ANOVA. Dunnett's test was then used to compare multiple groups with the control group. Two-sided t-tests were used to examine the statistical significance between two sample groups. Continuously distributed data were displayed by using box and whisker plots, with all elements (median, interquartile interval, minimum, maximum) presented in the figure, or by showing the data-points. The significance level was defined as $P < 0.05$, and significance tests were conducted using SAS 9.1 (SAS Institute).

Data availability

Data that support the findings of this study are available from the corresponding authors upon reasonable request.

Results

Characterization and neural differentiation of SPG11 iPSCs

In order to study the effects of perturbed spatacsin function on cortical neurons, we generated iPSCs from SPG11 patient-derived fibroblast cells. The episomal method, a non-integrating method,[30] was utilized to generate iPSCs by transducing fibroblast cells with episomal vectors containing pluripotent factors. Single clones were selected, and clones with typical pluripotent stem cell morphology were expanded for further characterization. These clones were positive for pluripotency markers OCT4, TRA-1-60, NANOG, and SSEA4 (Supplementary Fig. 1A and B). Normal karyotype was maintained following multiple passages (Supplementary Fig. 2). After these cells were injected into SCID mice, teratomas with
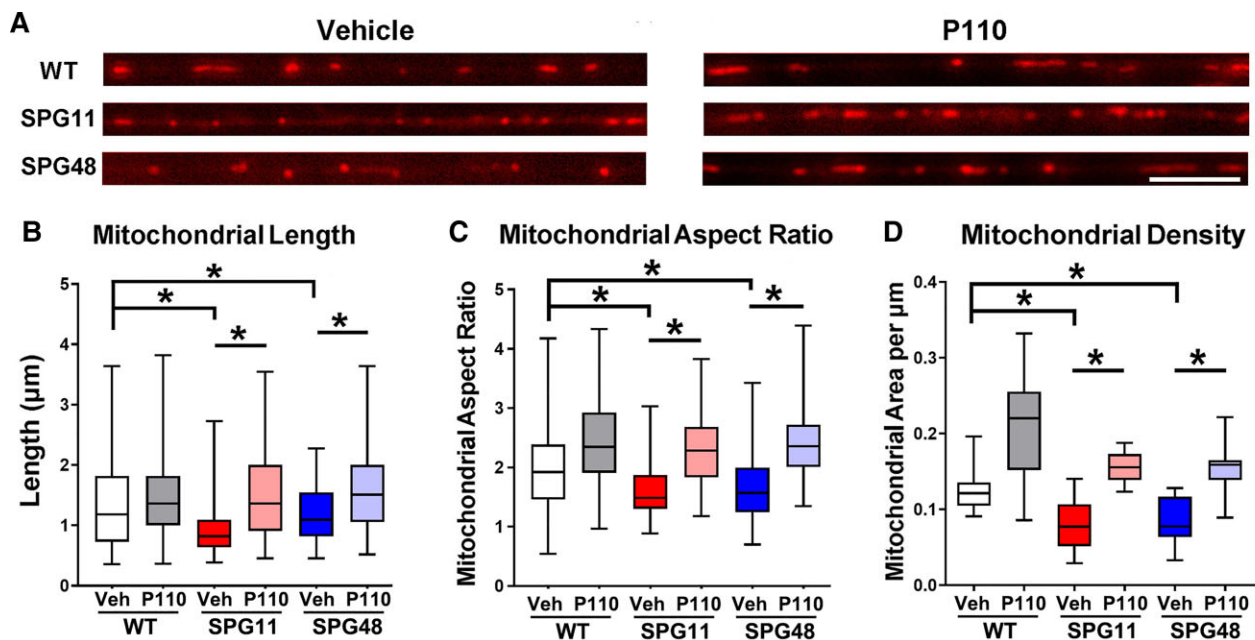
Figure 2 Mitochondrial fission inhibitor P110 restores mitochondrial morphology in SPG11 and SPG48 neurons. (**A**) Immunofluorescence images of mitochondria stained with MitoTracker within axons of wild-type (WT), SPG11 and SPG48 neurons, with or without P110 treatment. Scale bar = 10 μm. (**B**) Quantification of average mitochondrial length in wild-type, SPG11 and SPG48 neurons. A significant reduction of mitochondrial length in SPG11 and SPG48 neuron axons was mitigated with P110 treatment. (**C**) Average aspect ratio of mitochondria in wild-type, SPG11 and SPG48 neurons with or without P110 treatment. Data are presented using box and whisker plots (with median, interquartile interval, minimum, maximum) from a minimum of 110 mitochondria per group from three independent experiments. (**D**) Average linear mitochondrial density of wild-type, SPG11 and SPG48 neurons, with or without P110 treatment. A minimum of 15 axon segments were analysed per group in three independent experiments. Dunnett's test after ANOVA was used to compare multiple groups with the wild-type group. Two-sided t-tests were used to examine the statistical significance between vehicle- and P110-treated groups. *P < 0.05; n.s. = not significant.

typical three germ layer structures were formed, confirming the pluripotency of the iPSCs (Supplementary Fig. 1C). To validate the SPG11 mutations in these patient-specific iPSCs, we performed genomic DNA PCR and sequenced the relevant areas, confirming pathogenic compound heterozygous mutations of SPG11, c.3965delG and c.5769_5770dupT (Fig. 1A and B).

SPG11 iPSCs were differentiated into telencephalic glutamatergic neurons using protocols we have previously published.[32,33] Briefly, human iPSCs were detached from MEF feeder cells and formed aggregates in suspension to initiate spontaneous differentiation. These stem cell aggregates were then cultured in neural induction medium and formed adherent neuroepithelial cells. Next, SPG11 iPSCs were differentiated into neuroepithelial cells with uniform and characteristic columnar cell morphologies, suggesting efficient neural induction. These neural progenitor cells were isolated, expanded and plated for terminal differentiation of cortical projection neurons (Fig. 1C). Identities of cortical projection neurons were determined using the subcerebral neuron marker CTIP2[38] (Fig. 1C) and neuronal marker NeuN[39] (Supplementary Fig. 3A). SPG11 iPSCs differentiated into neural lineage and CTIP2+ cortical projection neuron efficiently, similar to control wild-type iPSCs (Supplementary Fig. 3B and C). The reduced expression of spatacsin at both mRNA and protein levels was confirmed in SPG11 iPSC-derived neural cultures (Supplementary Fig. 3D and E). Thus, spatacsin loss-of-function does not appear to affect the specification of cortical projection neuron. Interestingly, the axonal length of tau+ axons was significantly reduced in SPG11 compared to wild-type control neurons (Fig. 1D and E; vehicle-treated wild-type versus vehicle-treated SPG11 cells). The primary neurite length and number of branches

were also significantly reduced in SPG11 cortical neurons (Fig. 1F and G). Similar changes were observed in cortical neurons derived from SPG48 iPSCs (Fig. 1E–G); SPG48 is a rare, recessive HSP caused by loss-of-function of AP5Z1, a subunit of the heterotetrameric AP5 adaptor protein that is in complex with the SPG11 protein spatacsin and SPG15 protein spastizin. These data suggest that loss of spatacsin or AP5Z1 does not alter the neural lineage specification, but instead impairs axonal development at an early stage of differentiation.

Effects of P110 on axonal outgrowth of SPG11 and SPG48 cortical projection neuron

Our previous results demonstrated that Mdivi-1, an inhibitor of the Drp1 GTPase that mediates mitochondrial fission, can rescue axonal outgrowth defects in SPG15 and SPG48 neurons.[24] Here, we further examined whether mitochondrial defects underlie reduced axonal outgrowth in SPG11 cortical neurons and, more importantly, whether the dynamic process of axonal degeneration in these neurons can be rescued by targeting mitochondrial dynamics. We treated wild-type control and SPG11 neurons with P110, a potent and specific inhibitor for Drp1,[29] for 2 days, and then compared axon outgrowth with vehicle-treated cell groups (Fig. 1D–G). Our data show that axon length in SPG11 neurons is significantly increased after treatment with P110 as compared to the vehicle-treated SPG11 group (Fig. 1D and E). Similarly, the reduced primary neurite length in SPG11 cortical neuron axons was ameliorated after P110 treatment (Fig. 1F). Interestingly, P110 has no effect on the number of branches, suggesting that neurite branching and axonal elongation (length) are differentially regulated.
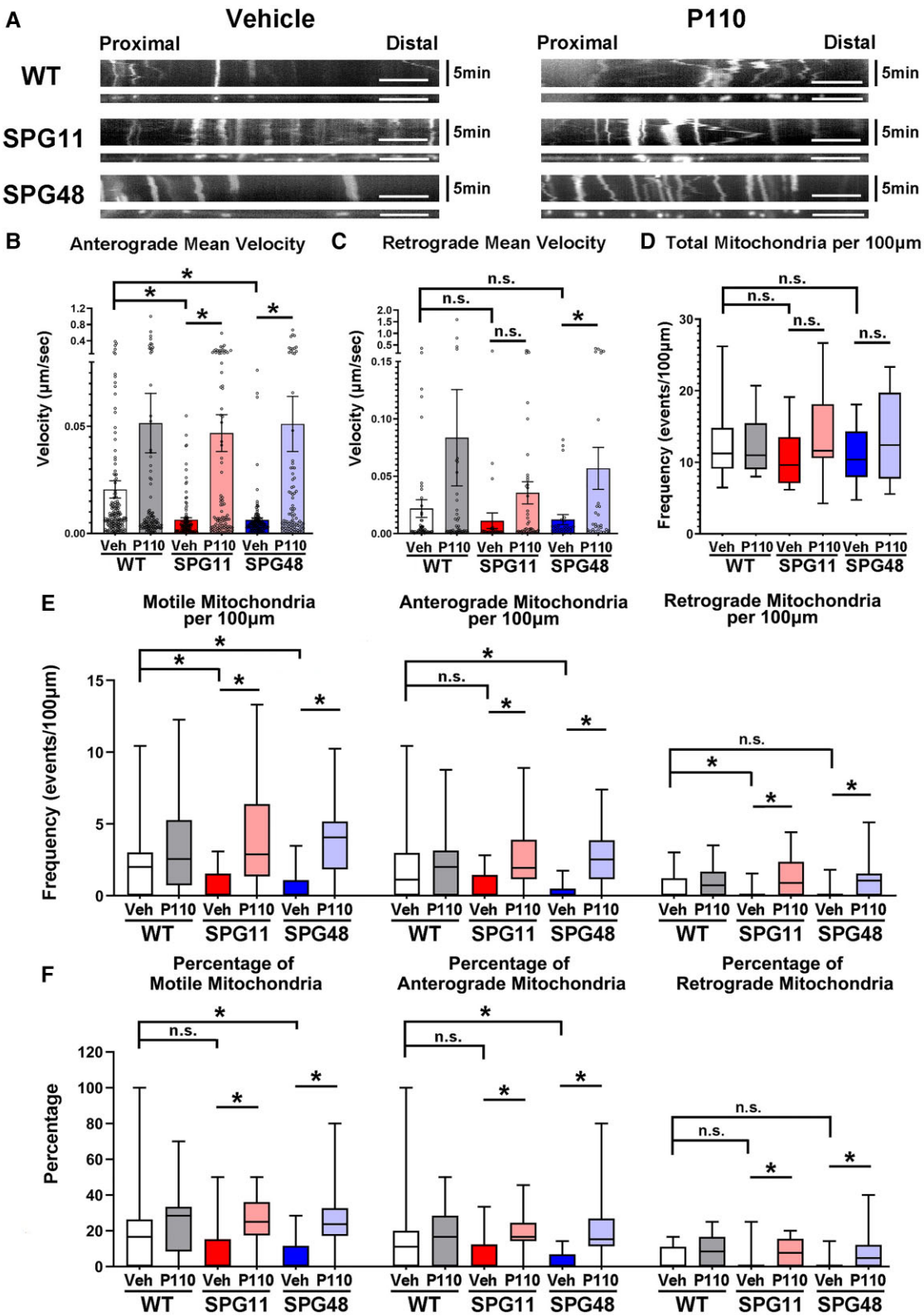
Figure 3 Mitochondrial fission inhibitor P110 improves mitochondrial motility in SPG11 and SPG48 neurons. (**A**) Representative distance (*x*-axis) versus time (*y*-axis) kymographs of motile mitochondria in axons of wild-type (WT), SPG11 and SPG48 neurons, with or without P110 treatment. *Bottom* images show relative Straighten results. Scale bar = 10 μm. (**B** and **C**) The velocity of mitochondria (at least 120 mitochondria per group from 15 axons) moving at anterograde or retrograde directions was examined. Quantifications of average anterograde velocities of mitochondria [means ± standard error of the mean (SEM)] show a significant reduction in SPG11 and SPG48 neurons as compared with wild-type neurons (**B**). This reduction is mitigated by P110 treatment. (**C**) Average mitochondrial retrograde velocities for wild-type, SPG11 and SPG48 neurons, with or without P110 treatment. (**D**) Quantification of total mitochondria number within 100 μm neurites of wild-type, SPG11 and SPG48 neurons. At least 15 axon segments

(Continued)

In order to examine the protective effects of P110 in other closely related recessive forms of HSP, we also treated SPG48 cortical neurons with P110 and tested whether their axonal outgrowth and later nerve degeneration can be modulated by P110. Though Mdivi-1 has been reported to affect mitochondrial respiration in addition to its Drp1-inhibiting effect,[40] P110 is a specific inhibitor for mitochondrial fission mediator, Drp1. SPG48 cortical neurons were treated with P110 for 2 days, the same treatment as for SPG11 cortical neurons (Fig. 1D–G). Similarly, P110 treatment significantly restores axon length (Fig. 1E) and neurite number (Fig. 1F) in SPG48 cortical neurons as compared to vehicle-treated groups. Together, these data suggest that P110 can effectively rescue early axonal outgrowth deficits in SPG11 and SPG48 cortical neurons.

P110 rescued abnormal mitochondrial morphology and mitochondrial moving ability in SPG11 and SPG48 neurons

Fast axonal transport of mitochondria is critical for maintaining normal axon functions, and it is regulated by mitochondrial dynamics.[41–44] Previous studies have shown that abnormalities in mitochondrial fission and fusion can lead to dysfunction in HSP neurons.[24] To examine defects in mitochondrial dynamics in SPG11 and SPG48, we treated these cortical projection neurons with mitochondrial fission inhibitor P110, a more specific mitochondrial fission inhibitor than Mdivi-1.[29,45,46] We first examined the effect of P110 on mitochondrial morphology in axons using live-cell imaging after MitoTracker dye staining, as previously described.[35] Average mitochondrial lengths in SPG11 and SPG48 axons are shorter than in wild-type neurons (Fig. 2A and B). Moreover, average mitochondrial lengths in SPG11 and SPG48 neurites treated with P110 are significantly increased as compared to that in vehicle group (Fig. 2A and B). P110 also significantly increases the mitochondria aspect ratio (length/width ratio) as well as mitochondrial densities in SPG11 and SPG48 axons (Fig. 2C and D). Similar protective effects are seen in SPG48 neurons upon treatment with P110, indicating that P110 is able to inhibit mitochondrial fission and rescue mitochondrial morphology abnormalities in SPG11 and SPG48 neurites.

We next asked whether P110 can improve mitochondrial motility in SPG11 and SPG48 axons. Wild-type, SPG11 and SPG48 cortical projection neurons were treated with P110 and then stained with MitoTracker™. Fluorescent images of axons in each group were taken every 5 s for a total of 5 min, and trajectories of individual mitochondria were acquired for representative kymograph analyses.[34] Decreased mitochondrial movement is observed in SPG11 and SPG48 vehicle groups as compared with the wild-type group, and treatment with P110 increases mitochondrial movement events in all groups (Fig. 3A and Supplementary Videos 1–6). Statistical analyses of trajectories from each mitochondrion reveals a significant reduction of anterograde mitochondrial moving velocity in axons of SPG11 and SPG48 vehicle groups compared with the wild-type group, and treatment with P110 restores mitochondrial motilities in SPG11 and SPG48 axons (Fig. 3B). The mitochondrial velocity in the retrograde direction shows a trend toward reduction, though no significant differences are observed between wild-type control

and SPG11 and SPG48 neurons (Fig. 3C), suggesting that anterograde transport is more affected, as reported in another study.[19] Although total mitochondria number per 100 µm has no significant differences across all groups (Fig. 3D), motile mitochondrial events are significantly reduced in SPG11 and SPG48 neurons compared to those in wild-type control neurons (Fig. 3E and F). Treatment with P110 significantly increases the mitochondrial frequencies and percentages in SPG11 neurons compared to vehicle-treated SPG11 neurons (Fig. 3E and F). Moreover, P110 ameliorates mitochondrial moving defects in SPG11 and SPG48 axons to levels similar to wild-type (Fig. 3E and F). These results indicate the mitochondrial moving ability and axonal transport of mitochondria in SPG11 and SPG48 axons are decreased and that applying P110 rescues these defects.

Inhibition of mitochondrial fission increased mitochondrial membrane potential and reduced neurofilament aggregation in SPG11 and SPG48 neuron axons

To examine the effects of P110 on mitochondrial health, we examined mitochondrial membrane potential in SPG11 and SPG48 neurons by incubating cells with TMRM, a fluorescent dye that binds mitochondria based on their membrane potentials.[47] After acquiring images of TMRM staining, the mitochondrial uncoupler FCCP (carbonylcyanide-*p*-trifluoromethoxyphenylhydrazone) was added to abolish TMRM staining, confirming the specificity of TMRM labelling.[47] A significant reduction of TMRM fluorescent intensity, which indicates decreased mitochondrial membrane potential, was observed in SPG11 and SPG48 neurons compared with wild-type neurons (Fig. 4A and B). Treatment with P110 increases TMRM fluorescence in both SPG11 and SPG48 neurons, indicating restoration of mitochondrial membrane potential and mitochondrial health (Fig. 4A and B). Addition of FCCP significantly reduced the fluorescent intensity, confirming that TMRM staining is dependent on mitochondrial membrane potential (Fig. 4C). To further investigate mitochondrial function, ATP levels within cells were measured using a luminescent ATP assay. Luminescence levels are significantly decreased in SPG11 and SPG48 neurons compared to wild-type control neurons, and this is partially restored after the treatment of P110 (Fig. 4D). Together, these data demonstrate that treatment with P110 rescues the reduced mitochondrial membrane potentials and ATP levels in SPG11 and SPG48 neurons, improving mitochondrial health and function.[48]

Mitochondrial membrane potential regulates the interaction between mitochondrial and neurofilaments, a type of intermediate filament important for axonal and neuronal function.[49] We examined whether the organization of neurofilaments is altered in HSP neurons and whether P110 has a role in this process. Cortical projection neurons derived from wild-type control, SPG11 and SPG48 iPSCs were stained with NFH200 antibody to examine the expression of neurofilament heavy chain (NFH) in neurons. In axons of both SPG11 and SPG48 neurons, we observed aggregations of NFH (Fig. 5A and B) and cell bodies (Fig. 5C). Interestingly, treatment with P110 dramatically reduced these aggregations (Fig. 5A–C). Quantifications reveal that numbers of NFH

Figure 3 Continued
were measured in each group. (**E**) Frequency of motile mitochondria (*left*), anterograde motile (*middle*) and retrograde motile (*right*) mitochondria per 100 µm in axons of wild-type, SPG11 and SPG48 neurons, with or without P110. (**F**) Quantifications showing percentages of motile (*left*), anterograde motile (*middle*) and retrograde motile (*right*) mitochondria among total mitochondria in axons of wild-type, SPG11 and SPG48 neurons, with or without P110 treatment. (**D–F**) Data are presented using box and whisker plots from a minimum of 15 axon segments analysed in three independent experiments. Dunnett's test after ANOVA was used to compare multiple groups with the wild-type group. Two-sided *t*-tests were used to examine statistical significance between vehicle- and P110-treated groups. *$P < 0.05$; n.s. = not significant.
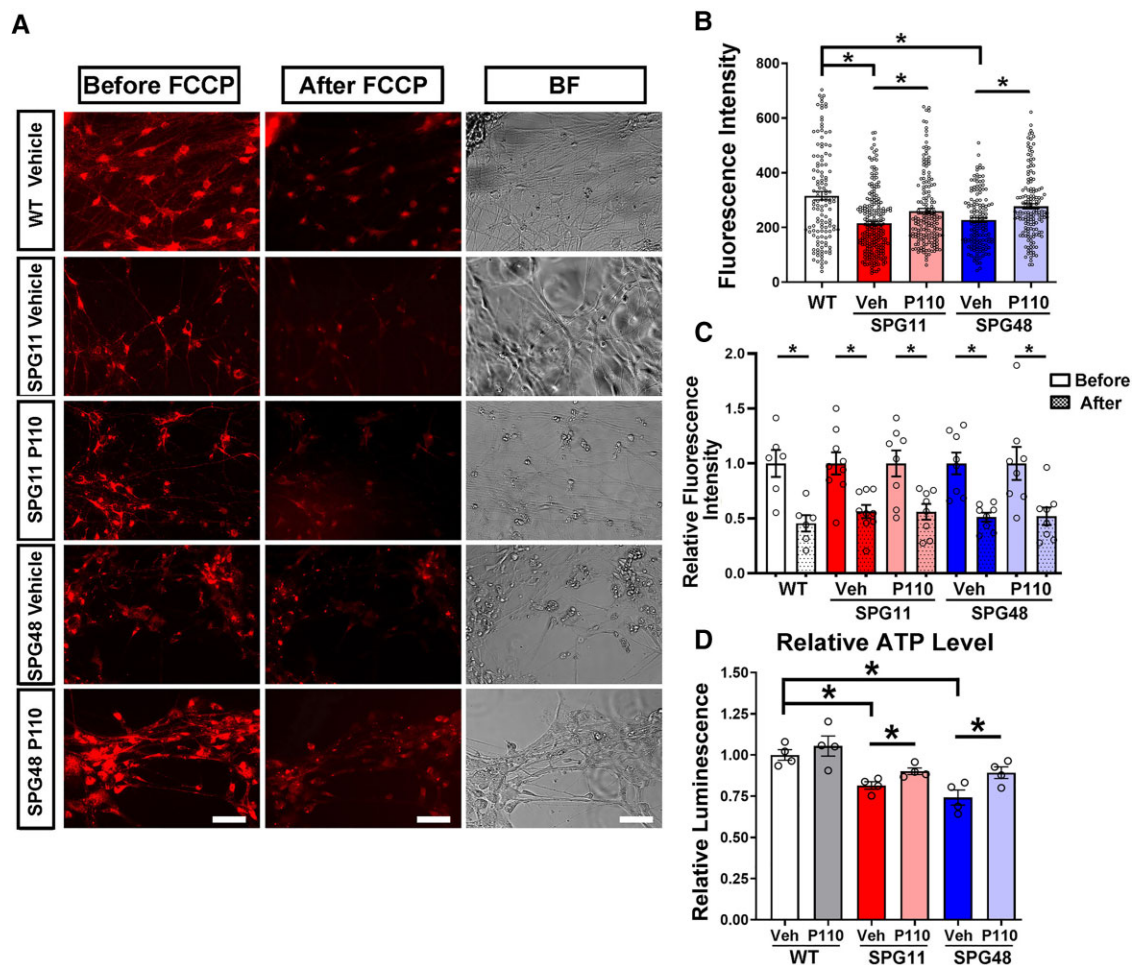
Figure 4 P110 rescues mitochondrial membrane potential in SPG11 and SPG48. (**A**) Images showing TMRM fluorescence before FCCP (*left*) and after FCCP treatment (*middle*). Bright field images from wild-type (WT), SPG11 and SPG48 neurons treated with vehicle or P110 are at the right. Scale bar = 50 μm. (**B**) Quantifications of TMRM fluorescence intensities for wild-type, SPG11 and SPG48 neurons, with or without P110 treatment. Data are presented as means ± SEM evaluating at least 100 neurons in three independent experiments. (**C**) Relative TMRM fluorescence intensities before and after FCCP treatment for wild-type, SPG11 and SPG48 neurons, with or without P110. $n = 6–9$ from three independent experiments. (**D**) ATP levels of wild-type, SPG11 and SPG48 neurons with or without P110 ($n = 4$) were measured using an ATP luminescence kit. Dunnett's test after ANOVA was used to compare multiple groups with wild-type group. Two-sided t-tests were used to examine the statistical significance between vehicle- and P110-treated groups (**B**) and before and after FCCP treatment (**C**). *$P < 0.05$; n.s. = not significant.

aggregations are significantly reduced after P110 treatment (Fig. 5B). Taken together, these data suggest that restoring normal mitochondrial dynamics can partially mitigate neurofilament aggregations, contributing to the protective effects of P110 in SPG11 and SPG48 neurons.

P110 mitigates neurofilament aggregations in cortical projection neurons derived from SPG11 and SPG48-knockdown hESCs

A common question in modelling disease-using iPSCs is whether the phenotypes observed are common across cells from different patients. HSP is a rare disease, and our previous study has shown that knockdown of the SPG48 protein AP5Z1 results in similar axonal defects.[24] Loss of gene function is a common mechanism underlying recessive forms of HSP. To confirm that axonal defects including aberrant neurofilament organization in SPG11 neurons are directly caused by loss of spatacsin function, we established SPG11 knockdown hESCs by combining lentivirus infection and RNA interference (Fig. 6A), a strategy we have used previously for

knocking down other genes in hESCs.[50] Two distinct shRNA sequences were utilized to knock down expression of SPG11 mRNA.

After establishing clonal SPG11 knockdown hESC lines, these SPG11-shRNA hESCs together with Luciferase-shRNA hESCs (as control) were differentiated into cortical projection neurons. CTIP2^{+} neurons were efficiently generated from SPG11 knockdown hESCs (GFP[+]) (Fig. 6B), suggesting that knockdown of *SPG11* does not affect the initial specification of cortical projection neuron. The mRNA expression of spatacsin is significantly decreased in both SPG11-shRNA#1 and SPG11-shRNA#2 groups at multiple stages during neural differentiation (Fig. 6C), confirming knockdown efficiency. Interestingly, in SPG11 knockdown cortical projection neuron, there is a significant increase in the neurofilament aggregations in both axons (Fig. 6D and E) and cell bodies (Fig. 6F and G), confirming that perturbed spatacsin causes neurofilament dysfunction. In *SPG11* knockdown neuronal cell bodies, Tom20-labelled mitochondria are observed in neurofilament aggregations, suggesting both abnormal mitochondria and neurofilament organization in these neurons (Fig. 6F and G). Interestingly, the increased number of neurofilament aggregations in SPG11-
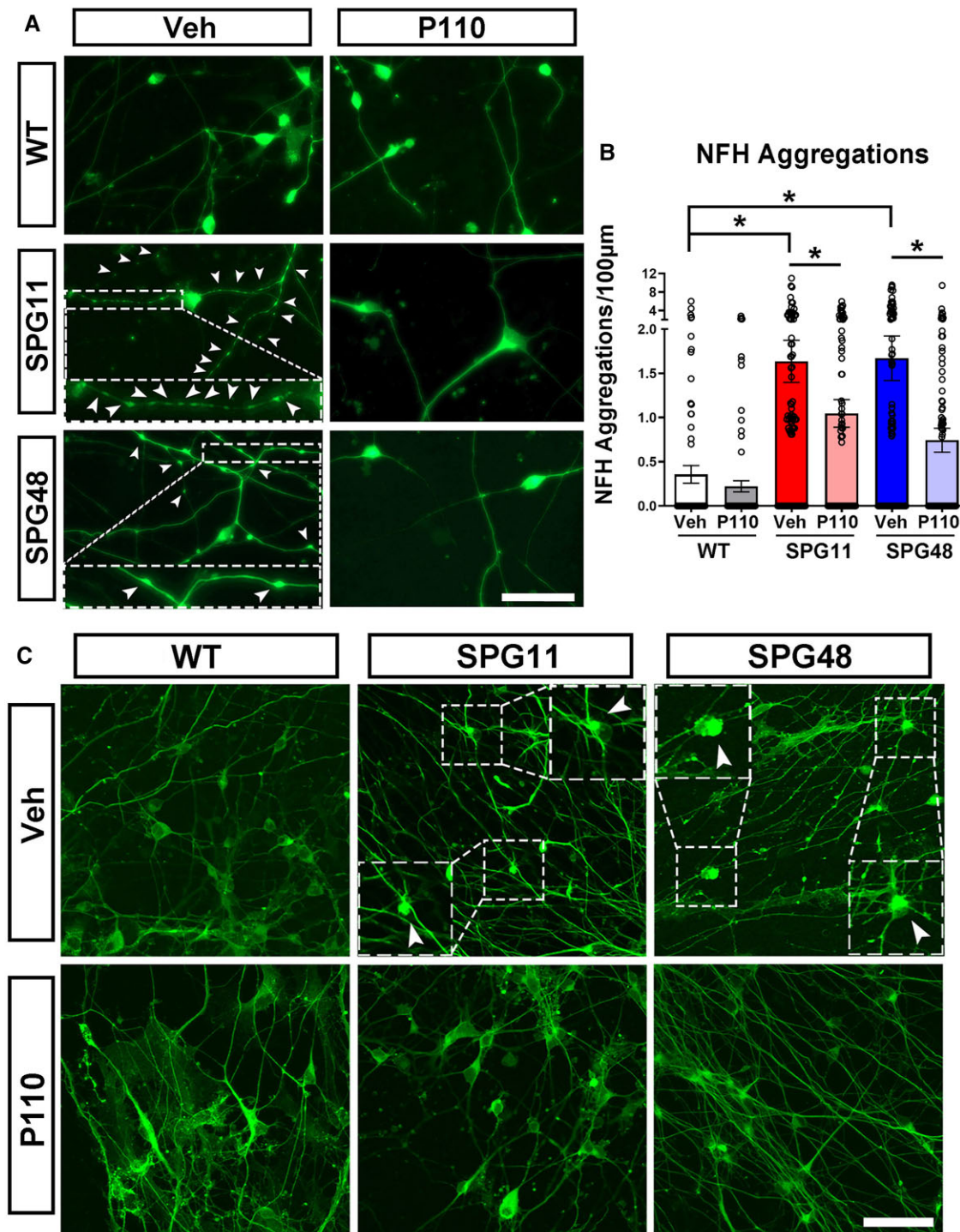
Figure 5 Effects of P110 on neurofilament aggregations in SPG11 and SPG48 neurons. (**A**) Immunostaining for NFH200 in wild-type (WT), SPG11 and SPG48 neurons, with or without P110 treatment. NFH aggregations (arrowheads) were observed in axons of SPG11 and SPG48 vehicle-treated neurons; enlargements at the *bottom* of the panels highlight neurofilament aggregations. (**B**) Quantifications of neurofilament aggregations in wild-type, SPG11 and SPG48 neurites, with or without P110 treatment. Data are presented as means ± SEM from at least 80 axon segments in three independent experiments. (**C**) Immunostaining of NFH200 in wild-type, SPG11 and SPG48 neurons shows aggregations (arrowheads) in cell bodies of SPG11 and SPG48 neurons. Enlarged areas highlight the neurofilament aggregations in these cell groups. Scale bars = 50 μm. Dunnett's test after ANOVA was used to compare multiple groups with wild-type group. Two-sided *t*-tests were used to examine the statistical significance between vehicle- and P110-treated groups. *$P < 0.05$.

knockdown cortical neuron axons and cell bodies is mitigated by targeting mitochondrial dynamics via P110 treatment (Fig. 6D–G).

Accumulation of neurofilament and protein aggregations is a pathological feature for amyotrophic lateral sclerosis,[51,52] a severe

motor neuron disease. Using post-mortem brain sections from SPG11 patients, a recent study reported the abnormal accumulation of granular lysosome-like structures and neurofilament aggregations as a hallmark pathology for SPG11.[13] Here, in SPG11 knockdown
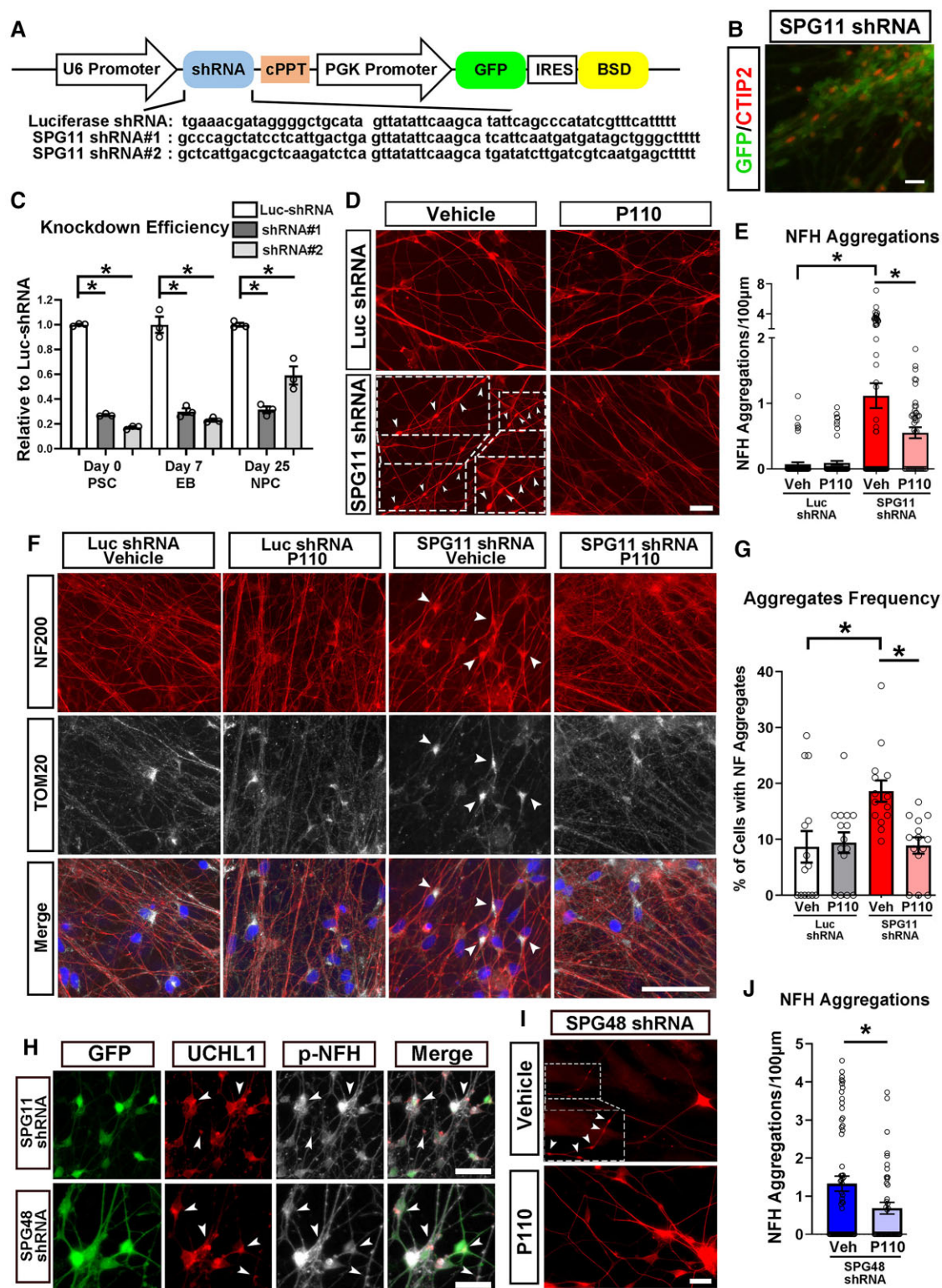
Figure 6 Knocking down *SPG11* and *AP5Z1* in cortical projection neurons increases neurofilament aggregation. (**A**) Schematic map of pLKO lentiviral vector containing shRNAs that target SPG11 (*SPG11*) or luciferase (as control). (**B**) Immunostaining images showing the generation of CTIP2^{+} cortical projection neurons from SPG11-RNAi hESCs. Scale bar = 20 μm. (**C**) Quantitative PCR showing mRNA expression of *SPG11* in cultures at different stages derived from SPG11- or Luciferase-shRNA hESCs ($n = 3$). (**D**) Immunostaining of NFH200 in shRNA-knockdown and control (Luciferase-shRNA) neurons treated with or without P110. NF-H aggregations (arrowheads) are observed in axons of SPG11 knockdown neurons, as highlighted in enlargements. Scale bar = 20 μm. (**E**) Quantifications of neurofilament aggregations in SPG11 shRNA and Luc shRNA neuron axons, with or without P110 treatment. At least 40 axon segments were measured in each group from three independent experiments. (**F**) Immunostaining of NFH200 and Tom20 showing the neurofilament and mitochondrial organization in cell bodies of cortical neurons derived from Luciferase-shRNA and SPG11-shRNA hESCs. Scale bar = 50 μm. (**G**) Quantifications reveal a significant increase in neurofilament aggregations in SPG11-knockdown neurons, which is mitigated by P110 treatment.

(Continued)

human cortical neurons, neurofilament aggregations also stain for ubiquitin C-terminal hydrolase L1 (UCHL1) (Fig. 6H), a ubiquitin and autophagy-related protein.[53,54] Double staining of neurofilament aggregation and UCHL1 (Fig. 6H) is also observed in cortical projection neuron derived from AP5Z1-knockdown hESCs that we previously established,[24] implying the involvement of neurofilament disorganization and protein degradation defects in both SPG11 and SPG48. Next, we examined the effects of P110 on SPG48 (AP5Z1)-knockdown cortical projection neuron. Similarly, as seen in SPG11 knockdown neurons, P110 significantly reduced neurofilament aggregations in AP5Z1 knockdown neurons (Fig. 6I and J). These data together suggest that SPG11 and SPG48 deficiencies result in neurofilament dysfunction and cytoskeletal disorganization in HSP, which can be rescued, at least partially, by applying P110 to inhibit mitochondrial fission.

Mitochondrial fission inhibitor P110 rescued axonal and neuronal degeneration in SPG11 and SPG48 long-term cultures

Phosphorylated neurofilament heavy chain protein (pNF-H) can accumulate along axons and be released from cells in neurodegenerative diseases, and thus can be used as a marker of neuronal degeneration.[55,56] To examine the nerve degeneration in long-term cultures, we first performed immunofluorescence staining of pNF-H in wild-type, SPG11 and SPG48 neurons at around 3 months after differentiation. We observed a significant increase in the number of pNF-H+ swellings in SPG11 and SPG48 axons compared to wild-type control group (Fig. 7A). Interestingly, after treatment with P110, the neurofilament-H aggregations are significant reduced in P110-treated neurons compared to those in vehicle-treated neurons (Fig. 7A and B). These data suggest that P110 can rescue axonal degeneration in long-term cultures of SPG11 and SPG48 cortical projection neuron.

Next, we measured the release of pNF-H in wild-type, SPG11 and SPG48 neurons after long-term culture (~3 months). The pNF-H released from degenerating neurons into the culture medium was measured with a pNF-H ELISA kit. Absorbance data show a significant reduction of pNF-H levels in P110-treated groups as compared with vehicle groups in SPG11 and SPG48 neurons (Fig. 7C). The correlation between the pNF-H in the media and cells suggests the usefulness of pNF-H release as a biomarker to monitor nerve degeneration in HSP. Furthermore, directly downregulating Drp1 by knocking down Drp1 expression with Drp1 shRNA (Fig. 7E) significantly reduces pNF-H levels in both SPG11 and SPG48 long-term cultures (Fig. 7F), confirming the rescue of nerve degeneration in these HSPs by targeting the mitochondrial fission mediator, Drp1. To examine whether neurons undergo apoptosis, we assessed levels of apoptosis in wild-type, SPG11 and SPG48 cells in long-term cultures (~15 weeks) using a caspase3/7 luminescence kit. Relative luminescence readouts showed that caspase3/7 levels in the SPG11 and SPG48 vehicle groups were significantly higher than in the wild-type vehicle group; treatment with P110 reduces levels of apoptosis in the SPG11 and SPG48 cells (Fig. 7D). These results indicate that P110 treatment decreases axonal swellings, release of pNF-H, and cell apoptosis in SPG11 and SPG48 neurons, effectively mitigating the axonal and neuronal degeneration of these neurons in long-term cultures.

Cause-effect relationship between the HSP gene mutations and disease phenotypes

To confirm that the HSP gene mutations directly cause the observed mitochondrial and neurofilament phenotypes, and to further examine the effects of P110, we generated SPG11 gene mutation (c.118C>T) knock-in hESC lines using CRISPR/cas9-mediated gene editing. Homozygous mutant clones were selected and confirmed by DNA Sanger sequencing (Supplementary Fig. 4A). This mutation leads to a premature stop codon at the 40th amino acid (p.Gln40X; the other base change from G to C at the 117 position facilitates gene editing and does not alter the amino acid sequence), which was reported in a SPG11 patient previously.[57] The reduced expression of spatacsin at both mRNA and protein levels was confirmed in the p.Gln40X hESC-derived neural cultures (Supplementary Fig. 4B and C). These p.Gln40X hESCs were then differentiated into CTIP2+ cortical projection neuron (Supplementary Fig. 4D). The proportion of CTIP2+ neurons was 79.5 ± 7.3%, comparable to H9 isogenic controls (77.8 ± 5.3%). Similarly, as seen in SPG11 iPSC-derived neurons, neurofilament-H aggregations are observed in p.Gln40X axons at 8 weeks (Supplementary Fig. 4E and F). ATP levels are also decreased in SPG11 p.Gln40X neurons as compared with H9 control neurons, revealing mitochondrial and neurofilament dysfunction caused by perturbed SPG11 (Supplementary Fig. 4G). Interestingly, after the treatment of P110, mitochondrial dysfunction and neurofilament aggregations in SPG11 p.Gln40X neurons are significantly mitigated (Supplementary Fig. 4H–J), further supporting the protective effects of P110 in SPG11 neurons.

Next, we performed rescue experiments by expressing wild-type spatacsin in both SPG11 patient iPSC- and p.Gln40X hESC-derived cortical neurons. Lentiviruses expressing SPG11-GFP (Lenti-SPG11) and GFP alone (Lenti-GFP, as a control) were generated and used to infect SPG11 iPSC- and SPG11 p.Gln40X hESC-derived neurons at 6 weeks. At 3 weeks after infection, cells were fixed for immunostaining or collected for measuring ATP levels. Successful viral infection was indicated by GFP fluorescence in these cells (Fig. 8A). Moreover, in the Lenti-SPG11 infected group, the expression of SPG11 is significantly increased compared to Lenti-GFP control group (Fig. 8B). After expressing wild-type spatacsin in these SPG11-deficient neurons, we found that the number of neurofilament-H aggregations is significantly decreased in both SPG11 iPSC and SPG11 p.Gln40X axons (Fig. 8C–F). Moreover, ATP levels in both SPG11 iPSC and SPG11 p.Gln40X neurons are significantly increased after expressing wild-type SPG11 (Lenti-SPG11) (Fig. 8G and H). The successful rescue of mitochondrial dysfunction and neurofilament aggregations in SPG11 neurons by expressing wild-type spatacsin supports a loss-of-function mechanism for SPG11 and demonstrates the cause-effect relationship between HSP mutations and disease phenotypes.

Discussion

How axons degenerate in HSP and how this dynamic process can be effectively targeted therapeutically to prevent or rescue the degeneration remain elusive. Here, we have examined the protective effects of targeting mitochondrial dynamics on axonal degeneration

Figure 6 Continued
At least 140 neurons were analysed in each group from three independent experiments. (**H**) Staining of pNF-H aggregations with UCHL1 in both SPG11 and SPG48 neurons. Scale bar = 50 µm. (**I** and **J**) In SPG48 (AP5Z1)-knockdown cortical projection neurons, P110 treatment significantly reduces the number of NFH aggregations along axons. A minimum of 40 axon segments were measured in each group from three independent experiments. Data are presented as means ± SEM. Scale bar = 20 µm. Dunnett's test after ANOVA was used to compare multiple groups with Luc-shRNA group (**C**), or compare with SPG11-shRNA Veh group (**E** and **G**). Two-sided *t*-tests were used to examine the statistical significance between vehicle- and P110-treated groups (**J**). *$P < 0.05$.
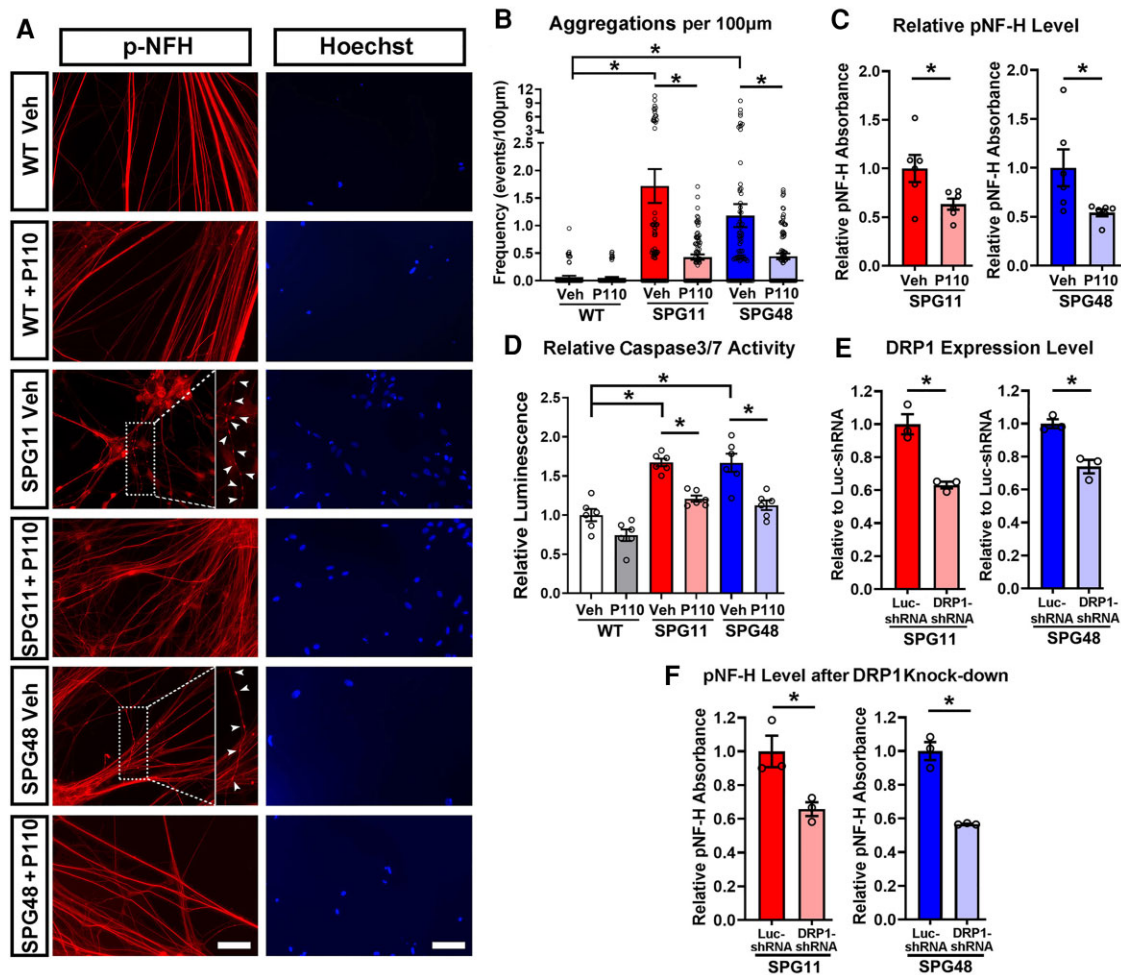
Figure 7 P110 treatment rescues axonal and neuronal degeneration in SPG11 and SPG48 cortical projection neurons. (**A**) Immunostaining of pNF-H in wild-type (WT), SPG11 and SPG48 neurites, with or without P110. Enlarged images show representative pNF-H aggregations. Arrowheads indicate swellings in axons. (**B**) Quantifications of pNF-H swellings in wild-type, SPG11 and SPG48 neurites, with or without P110. At least 70 neurites were measured in each group from three independent experiments. (**C**) Axonal injury levels revealed by pNF-H ELISA absorbance read-outs in SPG11 and SPG48 neurons with or without P110 treatment. (**D**) Apoptosis levels are indicated by caspase 3/7 activity, with luminescence read-outs in wild-type, SPG11 and SPG48 neurons with or without P110. (**E**) Drp1 shRNA knockdown efficiency was measured by qPCR. (**F**) To examine effects of Drp1 on release of pNF-H, SPG11 and SPG48 neurons were infected with lentiviruses containing Drp1 shRNA or Luciferase shRNA (Luc shRNA, as control), and media of these cultures were collected at one week after infection to analyse pNF-H. Data are presented as means ± SEM, $n = 3$. Dunnett's test after ANOVA was used to compare multiple groups with wild-type group. Two-sided t-tests were used to examine the statistical significance between vehicle- and P110-treated groups, and also between Luc-shRNA and Drp1-shRNA groups. *$P < 0.05$; n.s. = not significant.

in HSP subtypes SPG11 and SPG48. SPG11 and SPG48 patient-specific iPSC-derived cortical projection neurons recapitulate disease-specific axonal defects including reduced axonal outgrowth at an early-stage, reduced axonal transport, increased aggregation of neurofilament-H along axons, and upregulated release of phosphor-NFH in long-term cultures. Moreover, these patient iPSC-derived neurons exhibit mitochondrial defects including abnormal morphology (reduced length and aspect ratio), reduced motility, and decreased membrane potential. Treatment with P110 is able to restore normal mitochondrial morphology, increase mitochondrial mobility, improve mitochondrial health, and rescue axonal and neuronal degeneration in both SPG11 and SPG48 neurons. Directly targeting Drp1 by knocking down Drp1 expression using shRNA mitigated the increased release of pNF-H, a biomarker for axonal degeneration,[58,59] in long-term cultures. Thus, our study identifies protective effects of P110 against degeneration of human cortical neurons in SPG11 and SPG48, providing a therapeutic target

for SPG11 and SPG48 through modulating mitochondrial dynamics and cytoskeletal organization.

Neurons, especially long projection neurons, are highly energy demanding and depend on mitochondria to maintain normal function. Mitochondria are highly dynamic and undergo constant fission and fusion, which in turn regulates their morphology.[20,60] Abnormal mitochondrial morphology and dysregulated mitochondrial functions have been observed in several neurodegenerative diseases.[61,62] Using stem cell-based HSP models, we have identified reduced mitochondrial length in HSP cortical neurons,[24] which can be caused by increased mitochondrial fission, suggesting imbalanced mitochondrial fission/fusion in HSP. Indeed, the application of Mdivi-1, an inhibitor of Drp1, can restore mitochondrial morphology and rescue axonal outgrowth deficit.[24] Here, we have utilized P110, a specific inhibitor of Drp1, to examine the role of targeting mitochondrial dynamics in axonal degeneration at multiple stages during disease progression. P110 blocks the interaction between
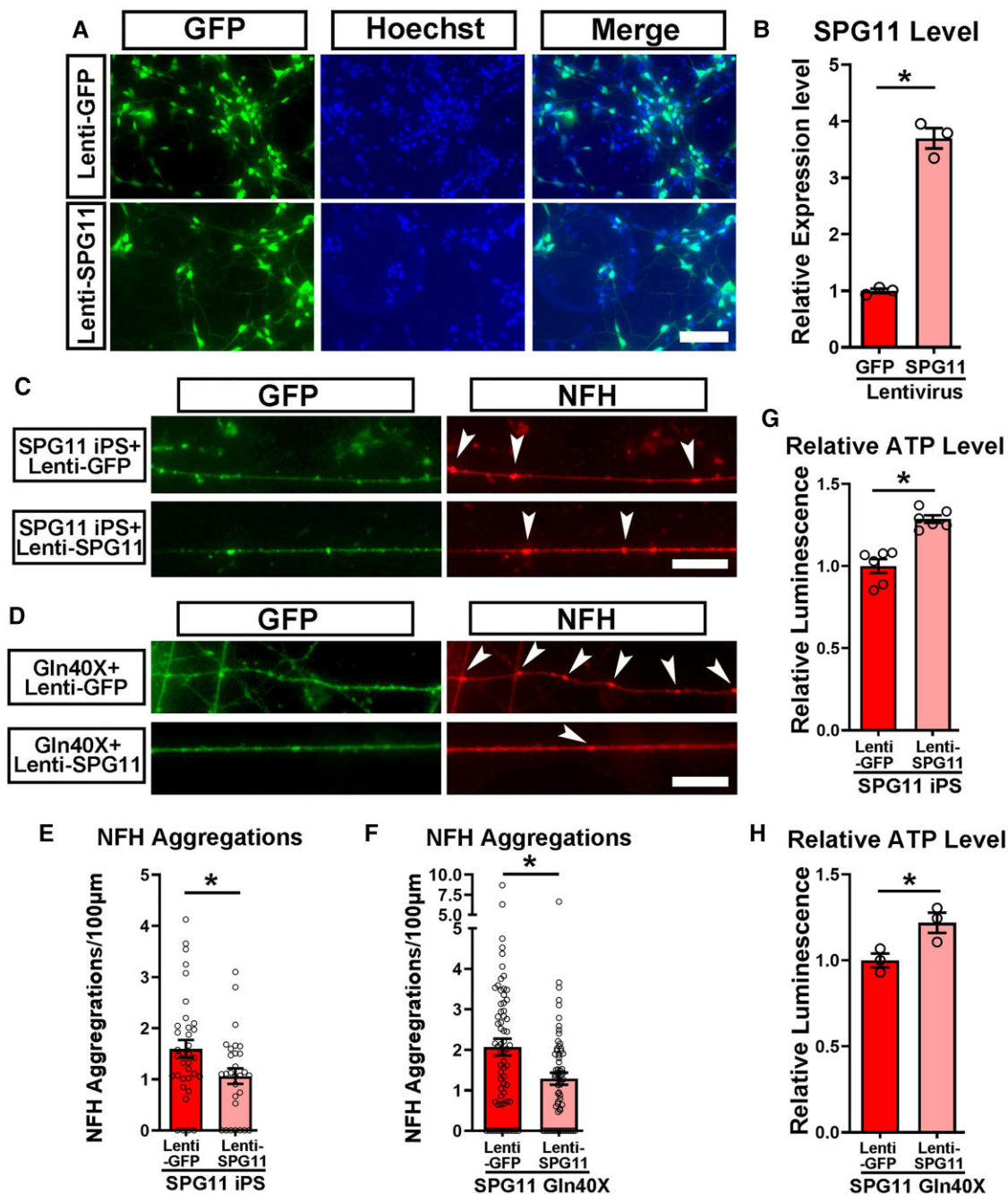
Figure 8 Expression of wild-type *SPG11* rescues mitochondrial defects in SPG11 iPSC and SPG11 p.Gln40X hESC. (**A**) Expression of GFP in SPG11 neurons indicates the successful infection of Lenti-GFP and Lenti-SPG11-GFP. Scale bars = 100 μm. (**B**) Quantitative PCR showing mRNA overexpression levels of *SPG11* in Lenti-GFP and Lenti-SPG11 neurons after 2-week infection ($n = 3$). (**C** and **D**) Immunostaining of NF-H in GFP positive neurites in SPG11 iPSC-derived neurons (**C**) and SPG11 p.Gln40X hESC-derived neurons (**D**) that were infected with lenti-GFP and lenti-SPG11. NF-H aggregations were indicated with arrowheads. Scale bars = 20 μm. (**E**) Quantifications of NF-H aggregations in GFP positive neurites in SPG11 iPSC-derived neurons. Data are presented as means ± SEM from ∼30 axon segments per group in three independent experiments. (**F**) Quantifications of NF-H aggregations in GFP positive neurites in neurons derived from p.Gln40X hESCs. At least 60 axon segments were measured in each group from three independent experiments. (**G**) After infection with lentiviruses containing full-length SPG11 (Lenti-SPG11) or GFP (Lenti-GFP, as controls), ATP levels in SPG11 iPSC-derived neurons were measured by ATP luminescence kit ($n = 6$). (**H**) Quantification of ATP levels in neurons derived from SPG11 p.Gln40X hESCs after infection with Lenti-GFP or Lenti-SPG11 lentiviruses ($n = 3$). Data are presented as means ± SEM. $*P < 0.05$ by two-sided *t*-test.

Drp1 and Fis1, two critical fission mediators, but does not disturb other Drp1 activity.[29] Though P110 has been used to reduce neuronal loss,[29] the effects of P110 on axonal degeneration have not been examined. Our data demonstrate that P110 can restore mitochondrial morphology, promote mitochondrial health, rescue impaired axonal transport, and mitigate increased aggregation and release

of NFH in long-term cultures. These data reveal the protective effects of P110 against axonal degeneration in HSP, providing a potential therapeutic agent for HSP.

How impaired mitochondrial dynamics result in axonal degeneration in HSP remains unclear. Accumulated axonal swellings and reduced mitochondrial transport are observed in SPG11 and SPG15

neurons, similar to reports for the most common HSP form SPG4[31,44]. Impaired axonal transport may cause accumulation of transported cargos and cytoskeleton proteins, leading to degeneration of axons. The detailed mechanisms and alterations of the transport machinery in HSP await further investigation. Specific changes in cortical projection neurons can be monitored by generating reporter lines that specifically label these neurons for testing axonal phenotypes. SPG11, SPG48, as well as SPG15, are autosomal recessive forms of HSP associated with autophagy and lysosomal defects, and they exist in a common multiprotein complex.[9,63,64] The reduced expression or absence of these HSP gene products combined with the rescue experiments from our previous[24] and current studies support a loss-of-function mechanism and suggest that normal levels of these proteins are critical for mitochondrial and axonal function. Endolysosomal and mitochondrial dysfunction can also affect one other in several common neurodegenerative diseases including Parkinson disease.[65] Thus, impaired mitochondrial dynamics in HSP may be secondary to endolysosomal and autophagy defects.

In addition to interacting with endolysosomes, mitochondria can interact with neurofilaments,[49] an important intermediate cytoskeleton for neurons and axons. Our data reveal increased aggregations of NFH in both cell bodies and axons of SPG11 and SPG48 neurons, implying disorganized neurofilaments in these HSPs. Moreover, release of pNF-H in long-term cultures in SPG11 and SPG48 neurons is significantly increased, which is mitigated by the downregulation of Drp1 both pharmacologically and genetically. The increased pNF-H provides a biomarker for monitoring axonal degeneration in HSP. Though the detailed interplay between impaired mitochondrial dynamics and cytoskeleton disorganization remains to be investigated, our study reveals that these impairments underlie axonal degeneration of human cortical neurons in SPG11 and SPG48, and they represent compelling targets for developing therapies to rescue axonal degeneration in these HSPs.

Funding

Competing interests

The authors report no competing interests.

Supplementary material

Supplementary material is available at *Brain* online.

References

1. Blackstone C, O'Kane CJ, Reid E. Hereditary spastic paraplegias: membrane traffic and the motor pathway. *Nat Rev Neurosci*. 2011;12(1):31–42.
2. Fink JK. Hereditary spastic paraplegia: clinico-pathologic features and emerging molecular mechanisms. *Acta Neuropathol*. 2013;126(3):307–328.
3. Finsterer J, Loscher W, Quasthoff S, Wanschitz J, Auer-Grumbach M, Stevanin G. Hereditary spastic paraplegias with autosomal dominant, recessive, X-linked, or maternal trait of inheritance. *J Neurol Sci*. 2012;318(1–2):1–18.
4. Blackstone C. Converging cellular themes for the hereditary spastic paraplegias. *Curr Opin Neurobiol*. 2018;51:139–146.
5. Hazan J, Fonknechten N, Mavel D, *et al*. Spastin, a new AAA protein, is altered in the most frequent form of autosomal dominant spastic paraplegia. *Nat Genet*. 1999;23(3):296–303.
6. Novarino G, Fenstermaker AG, Zaki MS, *et al*. Exome sequencing links corticospinal motor neuron disease to common neurodegenerative disorders. *Science*. 2014;343(6170):506–511.
7. Stevanin G, Azzedine H, Denora P, *et al*. Mutations in SPG11 are frequent in autosomal recessive spastic paraplegia with thin corpus callosum, cognitive decline and lower motor neuron degeneration. *Brain*. 2008;131(Pt 3):772–784.
8. Kara E, Tucci A, Manzoni C, *et al*. Genetic and phenotypic characterization of complex hereditary spastic paraplegia. *Brain*. 2016;139(Pt 7):1904–1918.
9. Hirst J, Borner GH, Edgar J, *et al*. Interaction between AP-5 and the hereditary spastic paraplegia proteins SPG11 and SPG15. *Mol Biol Cell*. 2013;24(16):2558–2569.
10. Pascual B, de Bot ST, Daniels MR, *et al*. "Ears of the Lynx" MRI sign is associated with SPG11 and SPG15 hereditary spastic paraplegia. *Am J Neuroradiol*. 2019;40(1):199–203.
11. Martin E, Yanicostas C, Rastetter A, *et al*. Spatacsin and spastizin act in the same pathway required for proper spinal motor neuron axon outgrowth in zebrafish. *Neurobiol Dis*. 2012;48(3):299–308.
12. Branchu J, Boutry M, Sourd L, *et al*. Loss of spatacsin function alters lysosomal lipid clearance leading to upper and lower motor neuron degeneration. *Neurobiol Dis*. 2017;102:21–37.
13. Denora PS, Smets K, Zolfanelli F, *et al*. Motor neuron degeneration in spastic paraplegia 11 mimics amyotrophic lateral sclerosis lesions. *Brain*. 2016;139(Pt 6):1723–1734.
14. Blackstone C. Cellular pathways of hereditary spastic paraplegia. *Annu Rev Neurosci*. 2012;35:25–47.
15. Salinas S, Proukakis C, Crosby A, Warner TT. Hereditary spastic paraplegia: clinical features and pathogenetic mechanisms. *Lancet Neurol*. 2008;7(12):1127–1138.
16. Stevanin G, Santorelli FM, Azzedine H, *et al*. Mutations in SPG11, encoding spatacsin, are a major cause of spastic paraplegia with thin corpus callosum. *Nat Genet*. 2007;39(3):366–372.
17. Słabicki M, Theis M, Krastev DB, *et al*. A genome-scale DNA repair RNAi screen identifies SPG48 as a novel gene associated with hereditary spastic paraplegia. *PLoS Biol*. 2010; 8(6):e1000408.
18. Mou Y, Li XJ. Rescue axonal defects by targeting mitochondrial dynamics in hereditary spastic paraplegias. *Neural Regen Res*. 2019;14(4):574–577.
19. Pérez-Brangulí F, Mishra HK, Prots I, *et al*. Dysfunction of spatacsin leads to axonal pathology in SPG11-linked hereditary spastic paraplegia. *Hum Mol Genet*. 2014;23(18):4859–4874.
20. Chan DC. Fusion and fission: interlinked processes critical for mitochondrial health. *Ann Rev Genet*. 2012;46:265–287.
21. Westermann B. Mitochondrial fusion and fission in cell life and death. *Nat Rev Mol Cell Biol*. 2010;11(12):872–884.
22. Labrousse AM, Zappaterra MD, Rube DA, van der Bliek AM. C. elegans dynamin-related protein DRP-1 controls severing of the mitochondrial outer membrane. *Mol Cell*. 1999;4(5):815–826.
23. Smirnova E, Griparic L, Shurland DL, van der Bliek AM, Pollard TD. Dynamin-related protein Drp1 is required for mitochondrial division in mammalian cells. *Mol Biol Cell*. 2001;12(8):2245–2256.
24. Denton K, Mou Y, Xu CC, *et al*. Impaired mitochondrial dynamics underlie axonal defects in hereditary spastic paraplegias. *Hum Mol Genet*. 2018;27(14):2517–2530.
25. Chamberlain SJ, Li XJ, Lalande M. Induced pluripotent stem (iPS) cells as in vitro models of human neurogenetic disorders. *Neurogenetics*. 2008;9(4):227–235.

26. Denton KR, Xu C, Shah H, Li XJ. Modeling axonal defects in hereditary spastic paraplegia with human pluripotent stem cells. *Front Biol.* 2016;11(5):339–354.

27. Ming GL, Brustle O, Muotri A, Studer L, Wernig M, Christian KM. Cellular reprogramming: recent advances in modeling neurological diseases. *J Neurosci.* 2011;31(45):16070–16075.

28. Weick JP, Meyer JS, Ladewig J, Guo W, Liu Y. Modeling CNS development and disease. *Stem Cells Int.* 2016;2016:3241057.

29. Qi X, Qvit N, Su YC, Mochly-Rosen D. A Novel Drp1 inhibitor diminishes aberrant mitochondrial fission and neurotoxicity. *J Cell Sci.* 2013;126(Pt 3):789–802.

30. Okita K, Matsumura Y, Sato Y, *et al.* A more efficient method to generate integration-free human iPS cells. *Nat Methods.* 2011;8(5):409–412.

31. Denton KR, Lei L, Grenier J, Rodionov V, Blackstone C, Li XJ. Loss of spastin function results in disease-specific axonal defects in human pluripotent stem cell-based models of hereditary spastic paraplegia. *Stem Cells.* 2014;32(2):414–423.

32. Boisvert EM, Denton K, Lei L, Li XJ. The specification of telencephalic glutamatergic neurons from human pluripotent stem cells. *J Vis Exp.* 2013;(74):50321.

33. Li XJ, Zhang X, Johnson MA, Wang ZB, Lavaute T, Zhang SC. Coordination of sonic hedgehog and Wnt signaling determines ventral and dorsal telencephalic neuron types from human embryonic stem cells. *Development.* 2009;136(23):4055–4063.

34. Denton KR, Xu CC, Li XJ. Modeling axonal phenotypes with human pluripotent stem cells. *Methods Mol Biol.* 2016;1353:309–321.

35. Mou Y, Mukte S, Chai E, Dein J, Li XJ. Analyzing mitochondrial transport and morphology in human induced pluripotent stem cell-derived neurons in hereditary spastic paraplegia. *J Vis Exp.* 2020;(156):10.3791/60548.

36. Errea O, Moreno B, Gonzalez-Franquesa A, Garcia-Roves PM, Villoslada P. The disruption of mitochondrial axonal transport is an early event in neuroinflammation. *J Neuroinflammation.* 2015;12:152.

37. Kang JS, Tian JH, Pan PY, *et al.* Docking of axonal mitochondria by syntaphilin controls their mobility and affects short-term facilitation. *Cell.* 2008;132(1):137–148.

38. Arlotta P, Molyneaux BJ, Chen J, Inoue J, Kominami R, Macklis JD. Neuronal subtype-specific genes that control corticospinal motor neuron development in vivo. *Neuron.* 2005;45(2):207–221.

39. Mullen RJ, Buck CR, Smith AM. NeuN, a neuronal specific nuclear protein in vertebrates. *Development.* 1992;116(1):201–211.

40. Bordt EA, Clerc P, Roelofs BA, *et al.* The putative Drp1 inhibitor mdivi-1 is a reversible mitochondrial complex I inhibitor that modulates reactive oxygen species. *Dev cell.* 2017;40(6):583–594.e6.

41. Tarrade A, Fassier C, Courageot S, *et al.* A mutation of spastin is responsible for swellings and impairment of transport in a region of axon characterized by changes in microtubule composition. *Hum Mol Genet.* 2006;15(24):3544–3558.

42. Ebbing B, Mann K, Starosta A, *et al.* Effect of spastic paraplegia mutations in KIF5A kinesin on transport activity. *Hum Mol Genet.* 2008;17(9):1245–1252.

43. Solowska JM, Morfini G, Falnikar A, *et al.* Quantitative and functional analyses of spastin in the nervous system: implications for hereditary spastic paraplegia. *J Neurosci.* 2008;28(9):2147–2157.

44. Kasher PR, De Vos KJ, Wharton SB, *et al.* Direct evidence for axonal transport defects in a novel mouse model of mutant spastin-induced hereditary spastic paraplegia (HSP) and human HSP patients. *J Neurochem.* 2009;110(1):34–44.

45. Joshi AU, Mochly-Rosen D. Mortal engines: Mitochondrial bioenergetics and dysfunction in neurodegenerative diseases. *Pharmacol Res.* 2018;138:2–15.

46. Reddy PH. Inhibitors of mitochondrial fission as a therapeutic strategy for diseases with oxidative stress and mitochondrial dysfunction. *J Alzheimers Dis.* 2014;40(2):245–256.

47. Joshi DC, Bakowska JC. Determination of mitochondrial membrane potential and reactive oxygen species in live rat cortical neurons. *J Vis Exp.* 2011;(51):2704.

48. Nicholls DG. Mitochondrial membrane potential and aging. *Aging Cell.* 2004;3(1):35–40.

49. Wagner OI, Lifshitz J, Janmey PA, Linden M, McIntosh TK, Leterrier JF. Mechanisms of mitochondria-neurofilament interactions. *J Neurosci.* 2003;23(27):9046–9058.

50. Wang ZB, Zhang X, Li XJ. Recapitulation of spinal motor neuron-specific disease phenotypes in a human cell model of spinal muscular atrophy. *Cell Res.* 2013;23(3):378–393.

51. Oberstadt M, Claßen J, Arendt T, Holzer M. TDP-43 and cytoskeletal proteins in ALS. *Mol Neurobiol.* 2018;55(4):3143–3151.

52. Xiao S, McLean J, Robertson J. Neuronal intermediate filaments and ALS: a new look at an old question. *Biochim Biophys Acta.* 2006;1762(11-12):1001–1012.

53. Costes S, Gurlo T, Rivera JF, Butler PC. UCHL1 deficiency exacerbates human islet amyloid polypeptide toxicity in beta-cells: evidence of interplay between the ubiquitin/proteasome system and autophagy. *Autophagy.* 2014;10(6):1004–1014.

54. Sala G, Marinig D, Arosio A, Ferrarese C. Role of chaperone-mediated autophagy dysfunctions in the pathogenesis of Parkinson's disease. *Front Mol Neurosci.* 2016;9:157.

55. Calvo AC, Manzano R, Atencia-Cibreiro G, *et al.* Genetic biomarkers for ALS disease in transgenic SOD1(G93A) mice. *PLoS One.* 2012;7(3):e32632.

56. Chen H, Qian K, Du Z, *et al.* Modeling ALS with iPSCs reveals that mutant SOD1 misregulates neurofilament balance in motor neurons. *Cell Stem Cell.* 2014;14(6):796–809.

57. Franca MC Jr, Yasuda CL, Pereira FR, *et al.* White and grey matter abnormalities in patients with SPG11 mutations. *J Neurol Neurosurg Psychiatry.* 2012;83(8):828–33.

58. Gendron TF, C9ORF72 Neurofilament Study Group, Daughrity LM, *et al.* Phosphorylated neurofilament heavy chain: A biomarker of survival for C9ORF72-associated amyotrophic lateral sclerosis. *Ann Neurol.* 2017;82(1):139–146.

59. Shaw G. The use and potential of pNF-H as a general blood biomarker of axonal loss: An immediate application for CNS injury. In: Kobeissy FH, ed. *Brain neurotrauma: Molecular, neuropsychological, and rehabilitation aspects.* CRC Press/Taylor & Francis; 2015.

60. Youle RJ, van der Bliek AM. Mitochondrial fission, fusion, and stress. *Science.* 2012;337(6098):1062–1065.

61. Chen H, Chan DC. Mitochondrial dynamics–fusion, fission, movement, and mitophagy–in neurodegenerative diseases. *Hum Mol Genet.* 2009;18(R2):R169–R176.

62. Magrané J, Cortez C, Gan WB, Manfredi G. Abnormal mitochondrial transport and morphology are common pathological denominators in SOD1 and TDP43 ALS mouse models. *Hum Mol Genet.* 2014;23(6):1413–1424.

63. Murmu RP, Martin E, Rastetter A, *et al.* Cellular distribution and subcellular localization of spatacsin and spastizin, two proteins involved in hereditary spastic paraplegia. *Mol Cell Neurosci.* 2011;47(3):191–202.

64. Chang J, Lee S, Blackstone C. Spastic paraplegia proteins spastizin and spatacsin mediate autophagic lysosome reformation. *J Clin Invest.* 2014;124(12):5249–5262.

65. Plotegher N, Duchen MR. Crosstalk between lysosomes and mitochondria in Parkinson's disease. *Front Cell Dev Biol.* 2017;5:110.